A new method reveals microtubule minus ends throughout the meiotic spindle

Kendra S. Burbank,[1,2] Aaron C. Groen,[2] Zachary E. Perlman,[2] Daniel S. Fisher,[1] and Timothy J. Mitchison[2]

[1]Department of Physics, Harvard University, Cambridge, MA 03138
[2]Department of Systems Biology, Harvard Medical School, Boston, MA 02115

Anastral meiotic spindles are thought to be organized differently from astral mitotic spindles, but the field lacks the basic structural information required to describe and model them, including the location of microtubule-nucleating sites and minus ends. We measured the distributions of oriented microtubules in metaphase anastral spindles in *Xenopus laevis* extracts by fluorescence speckle microscopy and cross-correlation analysis. We localized plus ends by tubulin incorporation and combined this with the orientation data to infer the localization of minus ends. We found that minus ends are localized throughout the spindle, sparsely at the equator and at higher concentrations near the poles. Based on these data, we propose a model for maintenance of the metaphase steady-state that depends on continuous nucleation of microtubules near chromatin, followed by sorting and outward transport of stabilized minus ends, and, eventually, their loss near poles.

Introduction

In this study, we investigate the localization of microtubule (MT) minus ends within the *Xenopus laevis* meiotic spindle. This localization is important because it may reflect the location of MT nucleation within the spindle. Since the discovery of centrosomes, models for the assembly and maintenance of mitotic and meiotic spindles have included a dominant role for spindle poles as MT nucleation centers (Wilson, 1937; Brinkley, 1985). The "search-and-capture" model suggested that poles dominate spindle morphogenesis, anchoring the minus ends of MTs, whereas plus ends polymerize and depolymerize until some are stabilized by kinetochores (Kirschner and Mitchison, 1986). Later models proposed that MTs could be stabilized "at a distance" by chromosomes, presumably via diffusible factors such as RanGTP (Dogterom et al., 1996; Hyman and Karsenti, 1996; Carazo-Salas and Karsenti, 2003).

In anastral spindles, which are typified by oocyte/egg meiotic spindles, centrosomes are unnecessary for spindle morphogenesis (Heald et al., 1996). Spindles assemble in an "inside-out" manner, with initial formation of MTs near chromatin, followed by condensation of minus ends into poles (Matthies et al., 1996; Gaglio et al., 1997; Endow and Komma, 1998; Sköld et al., 2005). In some meiotic spindles, density tapers off toward the poles in a manner suggesting that many MTs terminate before reaching the poles (Theurkauf and Hawley, 1992). Studies in X. laevis egg extracts, which recapitulate assembly of the anastral meiosis II spindle, show that chromosomes trigger an exchange of GTP on Ran, promoting MT nucleation in the absence of centrosomes, thereby probably explaining early steps in spindle assembly (for review see Gruss and Vernos, 2004). Continued production of RanGTP is also required for maintenance of the metaphase steady-state in anastral spindles (Mitchison et al., 2004; unpublished data), but it is unknown whether this is caused by stabilization or nucleation activity downstream. Steady-state anastral spindles might be dominated by nucleation at chromatin, like during assembly, or at poles assembled in response to Ran activation (Gruss et al., 2001; Nachury et al., 2001). Knowing the localization of nucleating sites is, thus, central to understanding spindle morphogenesis. The search-and-capture picture is based on spatial separation between nucleating and stabilizing centers, and new models would be required to account for morphogenesis by other mechanisms. To this end, we sought to measure the localization of minus ends within the spindle.

Previous work localized minus and plus ends using serial-section electron microscopy (McDonald et al., 1992; Ding et al., 1993; Mastronarde et al., 1993), but this method is difficult to apply to large spindles and lacks reliable markers for end polarity. MT ends nearest to centrosomes were assumed to be minus ends (McIntosh et al., 1979; Mastronarde et al., 1993; O'Toole et al., 2003), which is an unreliable criterion if MTs are nucleated throughout the spindle. "Hook decoration" (McIntosh and Euteneuer, 1984; Heald et al., 1997) allows

Correspondence to Kendra S. Burbank: burbank@fas.harvard.edu
Abbreviation used in this paper: MT, microtubule.
The online version of this article contains supplemental material.

The Journal of Cell Biology, Vol. 175, No. 3, November 6, 2006 369–375
http://www.jcb.org/cgi/doi/10.1083/jcb.200511112

identification of polarity, but is unsuitable for localizing ends because MTs elongate under the hook decoration conditions. γ-Tubulin complex is probably involved in nucleation, but our knowledge of its function is limited, so we cannot equate its localization with that of minus ends. NuMA and other spindle pole proteins probably move to the most distal minus ends in the spindle via dynein-mediated transport (Merdes et al., 2000). Instead of using any of these to locate minus ends, we developed a quantitative optical method combining analysis of oriented MT distributions with localization of plus ends by tubulin incorporation. Our analysis shows that MT minus ends are present everywhere in the spindle, with a minimum density near the chromosomes.

Results and discussion

Our method to calculate the density of plus and minus ends at a single location within a *X. laevis* extract spindle is shown in Fig. 1. Although we could not directly measure the density of minus ends, we could calculate the density of plus ends and the difference between the densities of plus and minus ends. The sum of these two quantities was the density of minus ends.

Our technique required three steps. First, to obtain the end densities, we observed the flow of MTs in a portion of the spindle (Fig. 1 A, i [dashed box]). The amounts of leftward and rightward flow were proportional to the local numbers of MTs with their minus ends toward each pole. Second, we looked at how the numbers of MTs varied in space to find the difference between the local densities of minus versus plus ends (Fig. 1 B). Third, we measured the local density of plus ends by observing incorporation of labeled tubulin into the spindle (Fig. 1 C). We summed the results of steps two and three to find the local density of minus ends. The process was repeated at many locations on the spindle-pole axis to find the spatial distributions of plus and minus ends.

Definitions

Throughout this paper, we rotate all spindles to be horizontal, then use "x" to denote position along the spindle-pole axis and "y" for the perpendicular direction.

We call MTs with plus ends to the left "left-pointing" and define "right-pointing" analogously. The "MT number," $N_L(x)$ or $N_R(x)$, is the number of left- or right-pointing MTs passing through a cross section of the spindle at point x. We can only measure $N_L(x)$ and $N_R(x)$ up to an unknown proportionally constant c. The "plus end density at x" is the number of plus ends present in a 1-μm-wide window around x. The minus end density is similarly defined. The "fractional plus end density," $e_+(x)$, is the fraction of MTs crossing x which have plus ends present in a 1-μm-wide window around x, i.e., the plus end density divided by $(N_L(x) + N_R(x))$. The fractional minus end density, $e_-(x)$, is similarly defined. We will show that we can calculate fractional densities with no unknown proportionality constants.

Measurement of the number of left- and right-pointing MTs

We first needed to find the number of left- and right-pointing MTs that passed through a spindle cross section at position x (Fig. 1 A). We determined orientation by using the fact that all

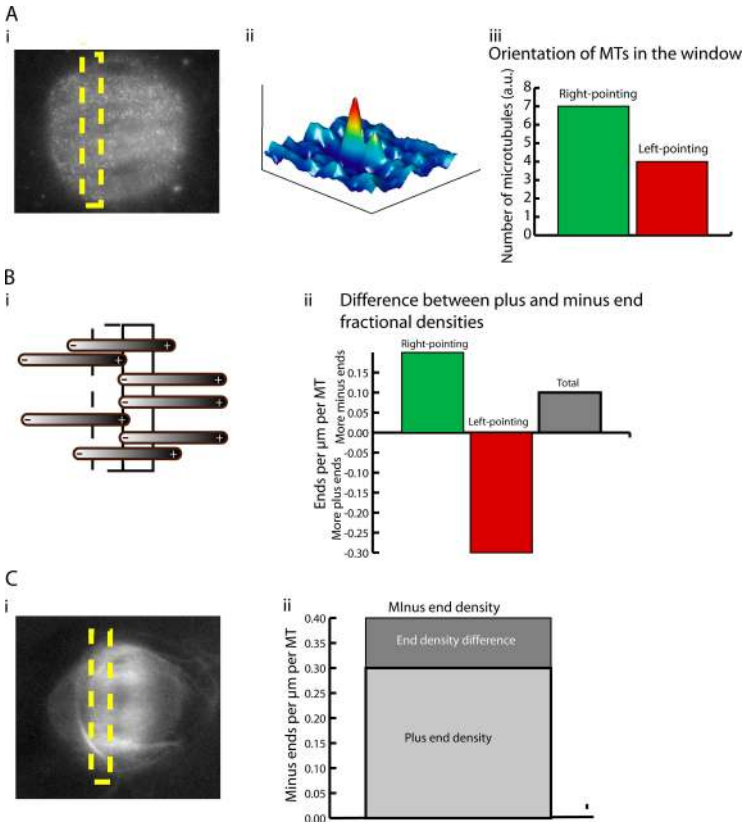

Figure 1. **Schematic of method for determining the fractional densities of plus and minus ends in a portion of the spindle.** (A) Measurement of the density of left- and right-pointing MTs. (i) Cross-correlation measures flow of speckles within the window (dashed box). The two peaks represent the flow toward each amount of the two poles. (ii) The volume of each peak gives the number of microtubules in the window fluxing in each direction. MTs moving left are assumed to have plus ends pointing right. (iii) Orientation of MTs in the window. (B) Calculation of the difference between fractional densities of plus and minus ends. (i) The number of right-pointing MTs is compared with the number in the adjacent window to the right. The change measures the difference in the number of plus versus minus ends in the window. This is because MTs with no ends in the two windows extend through both. MTs with plus ends extend only through the left window, while those with minus ends only through the right window. The difference between fractional densities of minus versus plus ends for left-pointing MTs is calculated in a similar manner, by comparing the number of left-pointing MTs with the number in the window to the left. The total difference is the sum of the left- and right-pointing differences. (ii) Difference between plus and minus end fractional densities. (C) Measurement of the density plus ends and calculation of the minus end fractional density. New tubulin incorporates into growing plus ends. The total number of plus ends in the window is found by measuring how quickly fluorescence intensity increases immediately after the addition of labeled tubulin. The fractional density of plus ends is added to the difference between plus and minus end fractional densities. This gives the fractional density of minus ends in the window. (ii) Fractional density of minus ends in the window.

MTs in *X. laevis* extract spindles are thought to slide continuously in the direction of their minus ends as they move poleward during metaphase. Leftward MT flow could thus be attributed to right-pointing MTs. We used speckle microscopy to visualize the sliding of MTs (Fig. 1 A, i) and cross-correlation (Westerweel, 1997; Miyamoto et al., 2004) to quantify the sliding in each direction (Fig. 1 A, ii). Thus, we obtained the number of left- and right-pointing MTs sliding through the window, up to an unknown proportionality constant, which was $c\ N_L(x)$ and $c\ N_R(x)$, respectively (Fig. 1 A, iii).

Fig. 2 shows examples of the number distributions of right- (solid lines) and left-pointing (dotted lines) MTs, which were plotted as functions of position along the spindle pole axis. These data represent 14 spindles from five extracts. The detailed distributions varied from spindle to spindle, reflecting the well-known variability in spindle morphology in the extract system, but the overall shapes were similar. The distributions agree with those calculated using the more precise, but computationally demanding, method of tracking and counting individual speckles (Vallotton et al., 2004; Fig. S1, available at http://www.jcb.org/cgi/content/full/jcb.200511112/DC1).

Calculation of the difference between the densities of plus and minus ends

We used the results from the previous step to find the difference in the local fractional densities of minus versus plus ends. We extracted this information from the spatial variations in the numbers of left- and right-pointing MTs (Fig. 1 B). To visualize how this was done, consider two adjacent windows in the spindle, and the number of right-pointing MTs in those windows (Fig. 1 B, i). A MT that does not terminate between the windows extends through both, thus, giving rise to no change in MT number. A minus end implies an increase in MT number moving from left to right, whereas a plus end implies a decrease. These effects are additive, so the MT number increases with x when minus ends outnumber plus ends. Thus, we found the difference in the densities of minus versus plus ends on right-pointing MTs by measuring their change in number from one window to the next. A similar analysis of the left-pointing MT numbers gave the difference in end densities for left-pointing MTs. The sum of these quantities, divided by the total number of MTs present, was the difference in fractional end densities for all MTs, $e_-(x) - e_+(x)$ (Fig. 1 B, ii). Mathematically, it is written as follows:

$$e_-(x) - e_+(x) = \left(\frac{d}{dx}\left(c\,N_R(x)\right) - \frac{d}{dx}\left(c\,N_L(x)\right)\right) \Big/ \left(c\,N_L(x) + c\,N_R(x)\right). \quad (1)$$

The unknown proportionality constant c cancels, so the fractional density difference is obtained in absolute units.

This analysis does not give the fractional densities of plus and minus ends separately, only the difference between them. Specifically, it cannot distinguish between a spindle made up of many short MTs, which would have a large number of both plus and minus ends, and a spindle with a smaller number of long MTs.

Measurement of the fractional plus end density

We needed an independent measurement of the fractional plus end density. We localized plus ends by pulsing labeled tubulin into extract and measuring its incorporation into preassembled spindles (Fig. 1 C, i). We assumed that tubulin is incorporated into MTs only at growing plus ends, so the initial rate at which florescence intensity increases is constant and proportional to the local density of plus ends (Supplemental materials and methods, available at http://www.jcb.org/cgi/content/full/jcb.200511112/DC1). From the rate of increase, we determined the fractional plus end density, $e_+(x)$. To visualize how this was done, imagine that the fractional plus end density is 0.2 ends per micrometer per MT and that 75% of all plus ends are growing. Thus, 15% of the MTs in a 1-μm-wide window have growing plus ends there. Assuming growth at the published rate of 10 μm/min (Verde et al., 1992), each of these ends will grow through the window in 6 s. Eventually, all MTs will be fully labeled. After 6 s, then, the intensity in the window will be 15% of its final value. We thereby calculated the 6-s fractional intensity increase to find the fraction of MTs with growing plus ends in the window. We divided this by the estimated ratio of growing to total plus ends, 0.75, to find the fractional density of all plus ends, growing or shrinking. Mathematically, it is written as follows:

$$e_+(x) = \frac{d}{dt}\left(I(x,t)\right)\Big|_{t=0} \Big/ \left(v_g\, f_g\, I(x,t)\right), \quad (2)$$

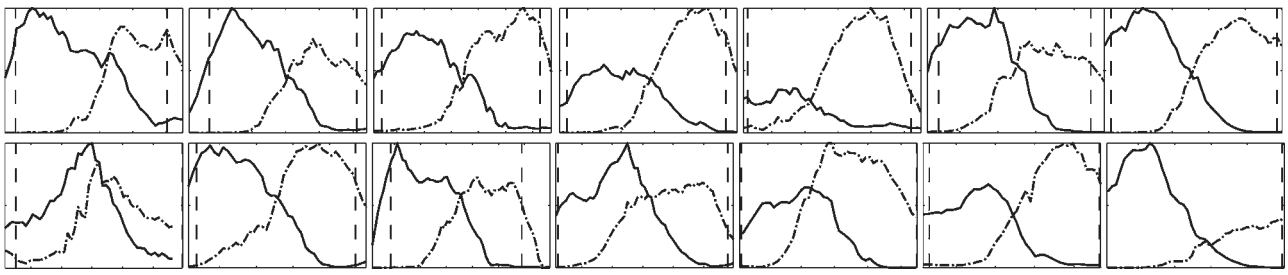

Figure 2. **Oriented MT number distributions.** Plots for 14 spindles showing oriented MT number distribution, in arbitrary units, versus position along the spindle-pole axis. Distributions for right-pointing MTs are given in solid lines, and distributions for left-pointing MTs are given in dotted lines. Spindle-pole positions, which were manually selected by the edge of visible florescence in spindle images, are marked with vertical dashed lines. The distance between tick marks on the x axis is 10 μm.

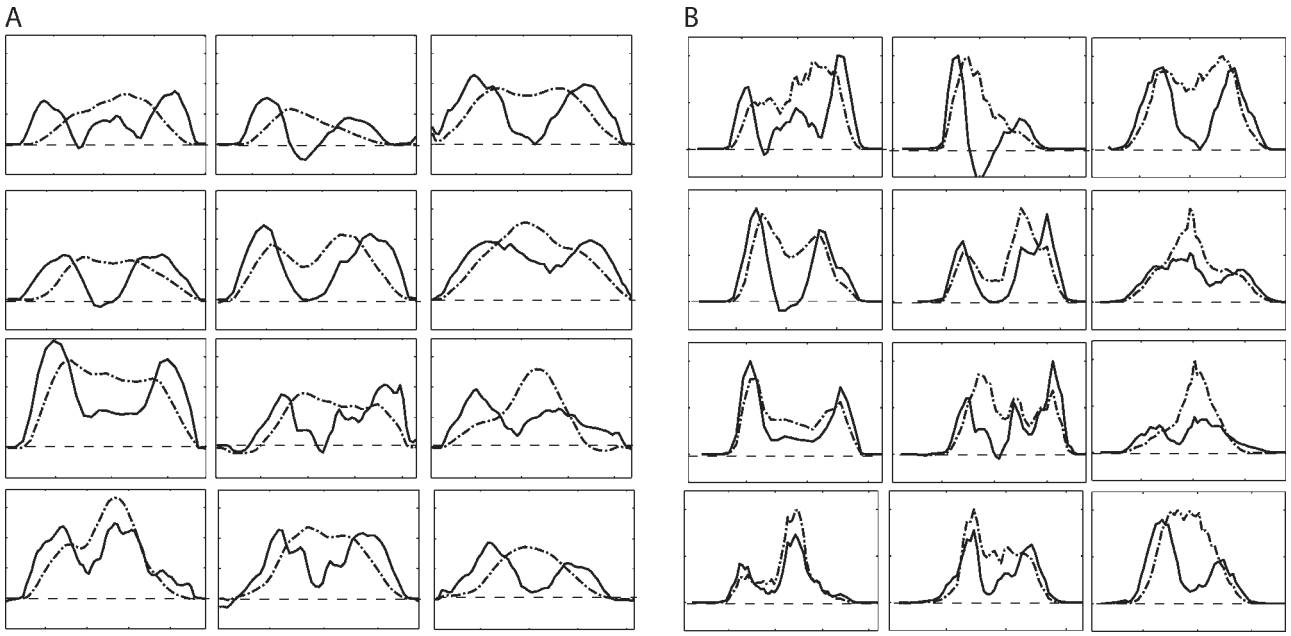

Figure 3. **Plus and minus end density distributions.** (A) A gallery of minus- (solid) and plus-end (dotted) fractional density distributions versus position along spindle-pole axis. The distance between tick marks on the x axis is 10 μm. Tick marks on the y axis represent 0.05 ends/μm, and dashed lines are at 0 ends/μm. (B) Plots of minus (solid) and plus end (dotted) density distributions, for the same spindles shown in A. X ticks represent 10 μm, and the y axes are in arbitrary units with dashed lines at 0.

where I(x,t) is the background-subtracted florescence intensity after summation in the y direction, at position x and time t after mixing. v_g is the plus end growth velocity, f_g is the fraction of plus ends which are growing, and t_f is the final time.

We found the densities and fractional densities of plus ends at each point along the spindle axis. Fig. 3 A (dotted lines) shows the distributions of fractional plus end densities from spindles assembled on four separate days, whereas Fig. 3 B shows the density distributions for the same spindles. Plus ends are broadly distributed throughout the center of the spindle, but their density drops sharply toward the poles.

The distributions were qualitatively similar to those obtained by imaging the tip-tracking protein EB1 (Tirnauer et al., 2004; unpublished data), but we chose to use the tubulin addition method because there was no way to calibrate the EB1 data to calculate the fractional plus end densities.

Averaging among spindles, we measured 0.08 plus ends per micrometer of MT, corresponding to an average MT length of ∼14 μm.

Calculation of the fractional minus end density

Our main goal in this study was to measure the localization of minus ends, for which we had no probe. Because at each position we now knew the difference between the fractional densities of plus and minus ends, and also the fractional density of plus ends from an independent measurement, we could calculate the fractional minus end density, $e_-(x)$, as the sum of these two numbers (Fig. 1 C, ii). The density was then given by $e_-(x)$ times the number of MTs.

In Fig. 3 (A and B), we show a gallery of minus end fractional density distributions (A, solid lines) and density distributions (B, solid lines). For each spindle, the minus end density was low at the equator and increased to broad peaks near the poles. The fractional density at the equator went as low as zero in spindles where antiparallel overlap was small, but was typically ∼0.1 minus end per micrometer per MT, rising to 0.2 minus ends per micrometer per MT at the peaks.

Conclusions

Our method provides the first way to optically localize MT ends of each polarity in an anastral spindle. It is currently the only way, as there is no reliable marker known for minus ends. Our analysis relies on two important assumptions; that all MTs moving left have their minus ends to the left, and that only plus ends incorporate new tubulin. The former is strongly expected from models in which motor proteins drive anastral spindle morphogenesis (Walczak et al., 1998; Miyamoto et al., 2004), but it has not been independently validated; if it is invalid, our method is not reliable. The latter assumption is supported by many observations of tubulin polymerization in cells, but also has not been independently validated for extract spindles. Our method has important limitations. It does not address kinetochore MTs, because these are very small in number compared with interpolar MTs, and all our measurements are bulk observations, not single MT data. For a more in-depth discussion of limitations, see the Supplemental materials and methods.

Because it depends on all spindle MTs sliding poleward, on speckle imaging, and on tubulin pulse labeling, our method cannot be applied to live somatic cells or eggs. However, *X. laevis* extract spindles provide a useful model for spindle assembly in general, and anastral morphogenesis in particular. Although their exact relevance to intact cell spindles can be debated, the mechanisms they have revealed have proven generally relevant.

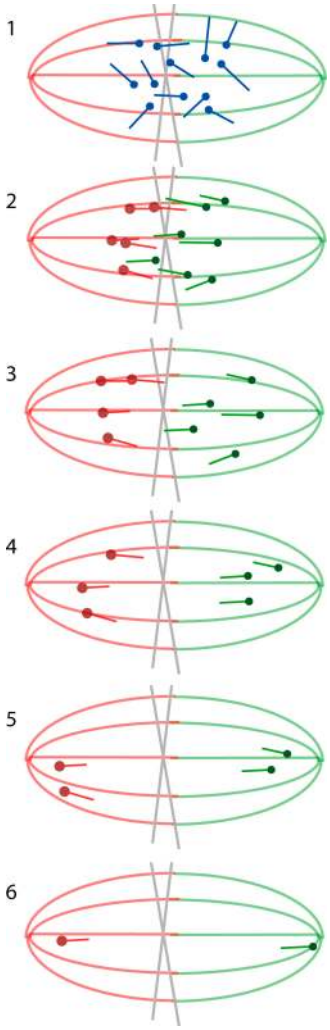

Figure 4. **Model of steady-state spindle formed by chromosomal nucleation and stochastic MT loss.** A steady-state spindle might be maintained through chromosomal nucleation, poleward sliding of MTs caused by the flux mechanism, and MT slowdown upon approach to the poles. (1) MTs are nucleated in a region around the chromosomes. (2) They initially point in random directions, but are sorted by motors to be parallel with the dominant MT orientation at the point of nucleation. (3–6) The MTs are moved poleward by a flux mechanism. Throughout the process, MTs and their minus ends disappear stochastically. As MTs disappear, new ones are continuously nucleated near the center.

We find that minus ends are localized in a distinctive manner within the spindle, with a deep trough near chromosomes, rising to a broad peak nearer the poles, then decreasing at or slightly before the poles (Fig. 3, A and B). This picture of a steady-state spindle with plus and minus ends distributed throughout has not been considered in any theoretical models. It is inconsistent with search-and-capture models (Kirschner and Mitchison, 1986) and computational models based on asters and motors (Nédélec, 2002) because minus ends are not located in discrete nucleating structures at poles.

The continued presence of minus ends throughout a spindle where all MTs are moving poleward implies either that minus ends are continuously produced in the center of the spindle by nucleation or severing, and then moved poleward, or that minus ends are static in position and depolymerize continuously; distinguishing between these alternatives requires a method for dynamic imaging of minus ends. We currently favor the moving end hypothesis for several reasons: TPX2, a Ran target implicated in MT nucleation, moves continually poleward at the flux rate, possibly in association with minus ends (Mitchison et al., 2004); Minus ends produced in S2 cell kinetochore fibers that are not attached to poles move toward the pole and only begin depolymerizing when they reach it (Maiato et al., 2005); and the Ran pathway, which can trigger MT nucleation, continues to operate in steady-state metaphase spindles, and there is no known reason nucleation near chromosomes should cease after spindles are assembled.

We favor a model in which maintenance of the metaphase steady-state in anastral spindles depends on continuous nucleation of MTs in a wide region around the chromosomes, followed by sorting and movement toward poles with minus ends neither polymerizing nor depolymerizing (Fig. 4). As existing minus ends are moved outward, they are joined at each point in the nucleation region by newly created ends, so their density increases from a minimum at the chromosomes. Other mechanisms, such as nucleation from the poles, may coexist with this process. The continuous nucleation proposed in this work is consistent with proposed functions of RanGTP (Carazo-Salas et al., 1999, 2001), but our data go a step further, emphasizing that Ran-driven nucleation is probably central to maintenance of the metaphase steady-state, as well as to initial spindle assembly. It is also consistent with recent observation of diffuse nucleation in S2 cells (Mahoney et al., 2006).

Our model makes testable predictions for the behavior of minus ends; because a single round of dynamic instability for a MT lasts, on average, ∼1 min, while reaching the pole from the chromosomes takes ∼8 min at the flux rate, minus ends would have to last for several cycles of dynamic instability. Our model then suggests a factor that stabilizes minus ends as they travel, possibly the same as the nucleator. To test this prediction, we need a reliable marker for minus ends that can be visualized optically, together with biochemical information on how MTs are nucleated—and how minus ends are transiently stabilized, if indeed they are—by the Ran pathway.

Materials and methods

Preparation and imaging of *X. laevis* extracts

We prepared *X. laevis* egg extracts and assembled spindles after one cycle of DNA replication (Desai et al., 1999). We performed florescence speckle microscopy (Waterman-Storer et al., 1998) using X-rhodamine–labeled tubulin (Invitrogen) at 25 μg/ml. Images were acquired at 20°C on a microscope (either E800 or 90i; Nikon) with 60×/1.4 NA or 100×/1.4 NA objectives (Plan Apo DIC; Nikon), immersion oil (Deltavision), and a cooled charge-coupled device camera (MicroMAX; Princeton Instruments [or ORCA-ER; Hamamatsu]) using Metamorph imaging software (Universal Imaging Corp.). 4–5 μl of spindle reactions were squashed under 18 × 18 mm coverslips and imaged by wide-field microscopy, with the focal plane in the middle of each spindle. We typically acquired 18 frames per spindle at 5-s intervals and 400-ms exposures.

Calculation of oriented MT number distributions

Each spindle was rotated to align its pole–pole axis with the x axis. Cross-correlations were calculated between sequential frames as a function of the x and y displacements Δx and Δy. These were averaged over the temporal sequence, as described in Miyamoto et al. (2004; Fig. 1 A, ii). A profile of the resultant surface was calculated along a line, near parallel with the

Δx axis, passing through the two peaks that represented leftward and rightward flow. To estimate the volumes of the two peaks, this profile was fit using Matlab (Mathworks) to a sum of two Gaussians plus a background term. The numbers of left- and right-pointing MTs were obtained from the integrated intensities under the peaks, up to an unknown proportionality constant (see Supplemental materials and methods).

Cross-correlations were found for windows 22 pixels wide (~3 μm), which were spaced every 1 μm along the length of the spindle, to obtain distributions of oriented MT number as a function of position (Fig. 2).

Calculation of fractional end fractional density differences

Oriented MT number distributions were smoothed in Matlab using a 20-pixel-wide moving-average filter. Left- and right-end number differences were obtained from the derivatives, computed moving left to right for right-pointing MTs and right to left for left-pointing MTs. The left and right end number differences were summed and then divided by the total MT number at each point to obtain the fractional end density difference. We focused on the midplane of each spindle, where the mean angle of MTs in the z direction was minimal, to minimize the effects of MTs entering or departing the plane of focus.

Plus end localization

3 μl of preformed spindles in extract that had been assembled with speckle-level X-rhodamine–labeled (red) tubulin were mixed on the slide with 2 μl of extract preequilibrated with 50 μg/ml green Alexa Fluor 488–labeled (Invitrogen) tubulin, squashed under a coverslip, and imaged as soon as possible (within 10–30 s) using a dry 40×/0.95 NA lens and ORCA-ER camera. After observation of incorporation of the green tubulin until near steady-state (~3 min), the objective was switched to a 60×/1.4 NA oil lens, and a speckle sequence of the same spindle was recorded for use in calculating oriented MT distributions. The median intensity, calculated in a region outside the spindle, was subtracted from each frame. New tubulin incorporation was measured as the intensity, recorded as a function of position along the spindle-pole axis (x) and the time elapsed after mixing (t), and summed along the direction perpendicular to the spindle-pole axis (y). At each point, the initial tubulin incorporation rate as a fraction of the final intensity was calculated from the increase of the intensity over the first 10 frames. This was divided by the published velocity of MT plus end growth, which was 10 μm/min (Verde et al., 1992), and the fraction of growing plus ends, 0.75 (Supplementary materials and methods), to obtain the fractional plus end density (Fig. 3 A, dotted lines). The fractional plus end densities were multiplied by the total MT number found from the cross-correlation to obtain plus end density distributions in the same (arbitrary) units as the latter (Fig. 3 B, dotted lines.) For more information, see Supplemental materials and methods.

Minus end localization

At each point, the fractional end density difference was added to the fractional plus end density to obtain the fractional density of minus ends (Fig. 3 A, solid lines.) Minus end density distributions, in arbitrary units, were found by multiplying the fractional density by the total MT number as calculated from cross-correlation analysis (Fig. 3 B, solid lines.)

Computer simulation

To test our analysis, we created data using Matlab, simulating MT creation, growth, shrinkage, flux, and the addition of labeled tubulin at a given time point. The images produced were analyzed using the same methods as for real data to calculate the distributions of plus ends, fractional end fractional density differences, and the distribution of minus ends. The calculated distributions agreed well with the real distributions (Supplemental materials and methods; Fig. S2, available at http://www.jcb.org/cgi/content/full/jcb.200511112/DC1).

Online supplemental material

The Supplemental materials and methods describe the calculation of dynamical cross-correlations, plus end density measurements and simulations, and internal consistency checks. Fig. S1 compares our cross-correlation method with the speckle-tracking method described in Vallotton et al. (2004) and frames from an image sequence of a spindle after green tubulin addition. Fig. S2 shows the results of the computer simulations to test the analysis techniques. Online supplemental material is available at http://www.jcb.org/cgi/content/full/jcb.200511112/DC1.

We would like to thank Ge Yang and Gaudenz Danuser for use of their speckle-tracking software and discussions about measurement of speckle flow, and Ryoma Ohi for suggesting the plus-end localization technique.

This work was supported by National Institutes of Health grants GM39565 and P50 GM068763-1. D.S. Fisher was supported in addition by the National Science Foundation via DMR-0229243.

Submitted: 28 November 2005
Accepted: 29 September 2006

References

Brinkley, B.R. 1985. Microtubule organizing centers. *Annu. Rev. Cell Biol.* 1:145–172.

Carazo-Salas, R.E., and E. Karsenti. 2003. Long-range communication between chromatin and microtubules in *Xenopus* egg extracts. *Curr. Biol.* 13:1728–1733.

Carazo-Salas, R.E., G. Guarguaglini, O.J. Gruss, A. Segref, E. Karsenti, and I.W. Mattaj. 1999. Generation of GTP-bound Ran by RCC1 is required for chromatin-induced mitotic spindle formation. *Nature*. 400:178–181.

Carazo-Salas, R.E., O.J. Gruss, I.W. Mattaj, and E. Karsenti. 2001. Ran-GTP coordinates regulation of microtubule nucleation and dynamics during mitotic-spindle assembly. *Nat. Cell Biol.* 3:228–234.

Desai, A., A. Murray, T.J. Mitchison, and C.E. Walczak. 1999. The use of *Xenopus* egg extracts to study mitotic spindle assembly and function in vitro. *Methods Cell Biol.* 61:385–412.

Ding, R., K.L. McDonald, and J.R. McIntosh. 1993. Three-dimensional reconstruction and analysis of mitotic spindles from the yeast, *Schizosaccharomyces pombe*. *J. Cell Biol.* 120:141–151.

Dogterom, M., M.A. Félix, C.C. Guet, and S. Leibler. 1996. Influence of M-phase chromatin on the anisotropy of microtubule asters. *J. Cell Biol.* 133:125–140.

Endow, S.A., and D.J. Komma. 1998. Assembly and dynamics of an anastral: astral spindle: the meiosis II spindle of Drosophila oocytes. *J. Cell Sci.* 111:2487–2495.

Gaglio, T., M.A. Dionne, and D.A. Compton. 1997. Mitotic spindle poles are organized by structural and motor proteins in addition to centrosomes. *J. Cell Biol.* 138:1055–1066.

Gruss, O.J., and I. Vernos. 2004. The mechanism of spindle assembly: functions of Ran and its target TPX2. *J. Cell Biol.* 166:949–955.

Gruss, O.J., R.E. Carazo-Salas, C.A. Schatz, G. Guarguaglini, J. Kast, M. Wilm, N. Le Bot, I. Vernos, E. Karsenti, and I.W. Mattaj. 2001. Ran induces spindle assembly by reversing the inhibitory effect of importin alpha on TPX2 activity. *Cell*. 104:83–93.

Heald, R, R. Tournebize, T. Blank, R. Sandaltzopoulos, P. Becker, A. Hyman, and E. Karsenti. 1996. Self-organization of microtubules into bipolar spindles around artificial chromosomes in *Xenopus* egg extracts. *Nature*. 382:420–425.

Heald, R., R. Tournebize, A. Habermann, E. Karsenti, and A. Hyman. 1997. Spindle assembly in *Xenopus* egg extracts: respective roles of centrosomes and microtubule self-organization. *J. Cell Biol.* 138:615–628.

Hyman, A.A., and E. Karsenti. 1996. Morphogenetic properties of microtubules and mitotic spindle assembly. *Cell*. 84:401–410.

Kirschner, M., and T. Mitchison. 1986. Beyond self-assembly: from microtubules to morphogenesis. *Cell*. 45:329–342.

Mahoney, N.M., G. Goshima, A.D. Douglass, and R.D. Vale. 2006. Making microtubules and mitotic spindles in cells without functional centrosomes. *Curr. Biol.* 16:564–569.

Maiato, H., A. Khodjakov, and C.L. Rieder. 2005. *Drosophila* CLASP is required for the incorporation of microtubule subunits into fluxing kinetochore fibres. *Nat. Cell Biol.* 7:42–47.

Mastronarde, D.N., K.L. McDonald, R. Ding, and J.R. McIntosh. 1993. Interpolar spindle microtubules in PTK cells. *J. Cell Biol.* 123:1475–1489.

Matthies, H.J., H.B. McDonald, L.S. Goldstein, and W.E. Theurkauf. 1996. Anastral meiotic spindle morphogenesis: role of the non-claret disjunctional kinesin-like protein. *J. Cell Biol.* 134:455–464.

McDonald, K.L., E.T. O'Toole, D.N. Mastronarde, and J.R. McIntosh. 1992. Kinetochore microtubules in PTK cells. *J. Cell Biol.* 118:369–383.

McIntosh, J.R., and U. Euteneuer. 1984. Tubulin hooks as probes for microtubule polarity: an analysis of the method and an evaluation of data on microtubule polarity in the mitotic spindle. *J. Cell Biol.* 98:525–533.

McIntosh, J.R., K.L. McDonald, M.K. Edwards, and B.M. Ross. 1979. Three-dimensional structure of the central mitotic spindle of *Diatoma vulgare*. *J. Cell Biol.* 83:428–442.

Merdes, A., R. Heald, K. Samejima, W.C. Earnshaw, and D.W. Cleveland. 2000. Formation of spindle poles by dynein/dynactin-dependent transport of NuMA. *J. Cell Biol.* 149:851–862.

Mitchison, T.J., P. Maddox, A. Groen, L. Cameron, Z. Perlman, R. Ohi, A. Desai, E.D. Salmon, and T.M. Kapoor. 2004. Bipolarization and poleward flux correlate during *Xenopus* extract spindle assembly. *Mol. Biol. Cell*. 15:5603–5615.

Miyamoto, D.T., Z.E. Perlman, K.S. Burbank, A.C. Groen, and T.J. Mitchison. 2004. The kinesin Eg5 drives poleward microtubule flux in *Xenopus laevis* egg extract spindles. *J. Cell Biol.* 167:813–818.

Nachury, M.V., T.J. Maresca, W.C. Salmon, C.M. Waterman-Storer, R. Heald, and K. Weis. 2001. Importin beta is a mitotic target of the small GTPase Ran in spindle assembly. *Cell*. 104:95–106.

Nédélec, F. 2002. Computer simulations reveal motor properties generating stable antiparallel microtubule interactions. *J. Cell Biol.* 158:1005–1015.

O'Toole, E.T., K.L. McDonald, J. Mäntler, J.R. McIntosh, A.A. Hyman, and T. Müller-Reichert. 2003. Morphologically distinct microtubule ends in the mitotic centrosome of *Caenorhabditis elegans*. *J. Cell Biol.* 163:451–456.

Sköld, H.N., D.J. Komma, and S.A. Endow. 2005. Assembly pathway of the anastral *Drosophila* oocyte meiosis I spindle. *J. Cell Sci.* 118:1745–1755.

Theurkauf, W.E., and R.S. Hawley. 1992. Meiotic spindle assembly in *Drosophila* females: behavior of nonexchange chromosomes and the effects of mutations in the *nod* kinesin-like protein. *J. Cell Biol.* 116:1167–1180.

Tirnauer, J.S., E.D. Salmon, and T.J. Mitchison. 2004. Microtubule plus end dynamics in *Xenopus* egg extract spindles. *Mol. Biol. Cell*. 15:1776–1784.

Vallotton, P., S.L. Gupton, C.M. Waterman-Storer, and G. Danuser. 2004. Simultaneous mapping of filamentous actin flow and turnover in migrating cells by quantitative fluorescent speckle microscopy. *Proc. Natl. Acad. Sci. USA*. 101:9660–9665.

Verde, F., M. Dogterom, E. Stelzer, E. Karsenti, and S. Leibler. 1992. Control of microtubule dynamics and length by cyclin A- and cyclin B-dependent kinases in *Xenopus* egg extracts. *J. Cell Biol.* 118:1097–1108.

Walczak, C.E., I. Vernos, T.J. Mitchison, E. Karsenti, and R. Heald. 1998. A model for the proposed roles of different microtubule-based motor proteins in establishing spindle bipolarity. *Curr. Biol.* 8:903–913.

Waterman-Storer, C.M., A. Desai, J.C. Bulinski, and E.D. Salmon. 1998. Fluorescent speckle microscopy, a method to visualize the dynamics of protein assemblies in living cells. *Curr. Biol.* 8:1227–1230.

Westerweel, J. 1997. Fundamentals of digital particle image velocimetry. *Meas. Sci. Technol.* 8:1379–1392.

Wilson, E.B. 1937. The Cell in Development and Heredity. 3rd edition. Macmillan, New York. 1232 pp.